NASA/CR—2003-212121

The Filtered Abel Transform and Its Application in Combustion Diagnostics

Zeng-Guang Yuan
National Center for Microgravity Research, Cleveland, Ohio

March 2003

The NASA STI Program Office . . . in Profile

Since its founding, NASA has been dedicated to the advancement of aeronautics and space science. The NASA Scientific and Technical Information (STI) Program Office plays a key part in helping NASA maintain this important role.

The NASA STI Program Office is operated by Langley Research Center, the Lead Center for NASA's scientific and technical information. The NASA STI Program Office provides access to the NASA STI Database, the largest collection of aeronautical and space science STI in the world. The Program Office is also NASA's institutional mechanism for disseminating the results of its research and development activities. These results are published by NASA in the NASA STI Report Series, which includes the following report types:

- TECHNICAL PUBLICATION. Reports of completed research or a major significant phase of research that present the results of NASA programs and include extensive data or theoretical analysis. Includes compilations of significant scientific and technical data and information deemed to be of continuing reference value. NASA's counterpart of peer-reviewed formal professional papers but has less stringent limitations on manuscript length and extent of graphic presentations.

- TECHNICAL MEMORANDUM. Scientific and technical findings that are preliminary or of specialized interest, e.g., quick release reports, working papers, and bibliographies that contain minimal annotation. Does not contain extensive analysis.

- CONTRACTOR REPORT. Scientific and technical findings by NASA-sponsored contractors and grantees.

- CONFERENCE PUBLICATION. Collected papers from scientific and technical conferences, symposia, seminars, or other meetings sponsored or cosponsored by NASA.

- SPECIAL PUBLICATION. Scientific, technical, or historical information from NASA programs, projects, and missions, often concerned with subjects having substantial public interest.

- TECHNICAL TRANSLATION. English-language translations of foreign scientific and technical material pertinent to NASA's mission.

Specialized services that complement the STI Program Office's diverse offerings include creating custom thesauri, building customized databases, organizing and publishing research results . . . even providing videos.

For more information about the NASA STI Program Office, see the following:

- Access the NASA STI Program Home Page at ***http://www.sti.nasa.gov***

- E-mail your question via the Internet to help@sti.nasa.gov

- Fax your question to the NASA Access Help Desk at 301–621–0134

- Telephone the NASA Access Help Desk at 301–621–0390

- Write to:
  NASA Access Help Desk
  NASA Center for AeroSpace Information
  7121 Standard Drive
  Hanover, MD 21076

NASA/CR—2003-212121

The Filtered Abel Transform and Its Application in Combustion Diagnostics

Zeng-Guang Yuan
National Center for Microgravity Research, Cleveland, Ohio

Prepared for the
1995 Fall Meeting, Western States Section
sponsored by The Combustion Institute
Stanford, California, October 30–31, 1995

Prepared under Cooperative Agreement NCC3–975

National Aeronautics and
Space Administration

Glenn Research Center

March 2003

Acknowledgments

The author gratefully acknowledges the help from Dr. David Urban (NASA Glenn), in the entire course of this study, and the help from Paul Greenberg (NASA Glenn), and Paul Ferkul (Analex Corp.), for their valuable suggestions when the manuscript was reviewed. The author would like to thank Dr. Uday Hegde (NYMA, Inc.), for his encouragement in the preparation of this paper, Dr. Fletcher Miller (Case Western Reserve University), for informative discussions on the subject, and Robert Klimec for implementing the described method in an in-house software. This study was supported by the Physical Sciences Research Division of the NASA Office of Biological and Physical Research.

Available from

NASA Center for Aerospace Information
7121 Standard Drive
Hanover, MD 21076

National Technical Information Service
5285 Port Royal Road
Springfield, VA 22100

Available electronically at http://gltrs.grc.nasa.gov

The Filtered Abel Transform and Its Application in Combustion Diagnostics

Zeng-Guang Yuan
National Center for Microgravity Research
Cleveland, Ohio 44135

Abstract

Many non-intrusive combustion diagnostic methods generate line-of-sight projections of a flame field. To reconstruct the spatial field of the measured properties, these projections need to be deconvoluted. When the spatial field is axisymmetric, commonly used deconvolution methods include the Abel transform, the onion peeling method and the two-dimensional Fourier transform method and its derivatives such as the filtered back projection methods. This paper proposes a new approach for performing the Abel transform numerically, which avoids the derivative calculation of the projection data. In addition, a new filtered Abel transform method is developed, which possesses the exactness of the Abel transform and the flexibility of incorporating various filters in the reconstruction process.

The Abel transform is an exact method and the simplest among these commonly used methods. It is evinced in this paper that all the exact reconstruction methods for axisymmetric distributions must be equivalent to the Abel transform because of its uniqueness and exactness. Detailed proof is presented to show that the two dimensional Fourier methods when applied to axisymmetric cases is identical to the Abel transform. Discrepancies among various reconstruction methods stem from the different approximations made to perform numerical calculations.

An equation relating the spectrum of a set of projection data to that of the corresponding spatial distribution is obtained, which shows that the spectrum of the projection is equal to the Abel transform of the spectrum of the corresponding spatial distribution. From this equation, if either the projection or the distribution is bandwidth limited, the other is also bandwidth limited, and both have the same bandwidth. If the two are not bandwidth limited, the Abel transform has a bias against low wave number components in most practical cases. This explains why the Abel transform and all exact deconvolution methods are sensitive to high wave number noises.

The filtered Abel transform is based on the fact that the Abel transform of filtered projection data is equal to an integral transform of the original projection data with the kernel function being the Abel transform of the filtering function. The kernel function is independent of the projection data and can be obtained separately when the filtering function is selected. Users can select the best filtering function for a particular set of experimental data. When the kernel function is obtained, it can be used repeatedly to a number of projection data sets (rows) from the same experiment. When an entire flame image that contains a large number of projection lines needs to be processed, the new approach significantly reduces computational effort in comparison with the conventional approach in which each projection data set is filtered and deconvoluted separately.

Computer codes have been developed to perform the filtered Abel transform for an entire flame field. Measured soot volume fraction data of a jet diffusion flame are processed as an example.

I. Introduction

A large portion of combustion research effort has been devoted to the study of axisymmetric flame fields. Examples include laminar jet flames, both premixed and diffusion, spherical flames in premixed gases, and flames surrounding liquid or solid fuel droplets. Many non-intrusive diagnostic methods are available to provide line-of-sight projection data of various important parameters in the flame region. For instance, laser extinction for soot volume fraction measurement, emission/absorption thermometry for sooting flame temperature, IR emission for flame temperature measurement, and laser extinction/scattering for soot particle size measurement have been reported [1-5]. Figure 1 illustrates the relation between the projection and the spatial distribution of a flame property in a plane normal to the streamwise axis of an axisymmetric flame. The projection function p(l) is related to the line-of-sight integration of the flame property f(r) by the following equation:

$$p(l) = \int_{-\infty}^{\infty} f(r)\, ds \qquad (1)$$

With a large number of simultaneous projection lines, an entire flame image can be obtained instantly. For example, full field laser extinction for soot volume fraction [6] and full field two wave lengths soot pyrometry acquire instantaneous 2-D flame images.

It is a crucial step in experimental data reduction to reconstruct the spatial distribution of the flame property based on the measured line-of-sight projections. This requires the inversion of Eq. (1). Many methods for the

reconstruction of axisymmetric distributions have been reported. Among them the Abel transform, reported in 1826 [7], gives a concise, exact solution for the reconstruction. Other commonly used methods are "onion-peeling" and filtered back projection (FBP). The "onion-peeling" method is directly based on numerical approximation. Its efficiency decreases as the number of data points increases. The FBP method was derived from the two dimensional Fourier transform method and originally developed for two dimensional X-ray tomography [8,9]. Owing to its success in medical applications, it was introduced to study flame and flow fields of both non-axisymmetric cases [1,2,4] and axisymmetric cases [3,5,10], assuming angular independence of the projections in the latter.

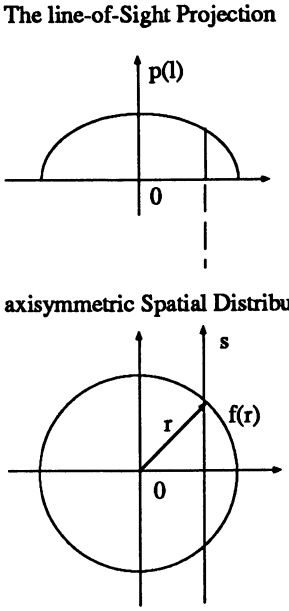

Figure 1. The line-of-sight integration of an axisymmetric spatial distribution.

This paper evinces that both the onion-peeling method, in the limiting condition, and the two dimensional Fourier transform method when used for axisymmetric cases are identical to the Abel transform method. An alternative form of the Abel equation is suggested to perform numerical calculations that avoids calculating derivatives of the projection data, thus simplifying the algorithms and eliminating errors caused by derivative calculations. In addition, the spectral behavior of the Abel transform is discussed. It is shown that the Abel transform exhibits a bias towards high wave number components. This accounts for the rugged results from the Abel transform when it is directly applied to experimental data. Instead of performing filtering and reconstruction separately, a new method, the filtered Abel transform, is developed which adds data filtering features to the Abel method. The filtered Abel transform is found to be efficient when a large number of data points needs to be processed, for example, when processing a full flame image.

II. The Abel transform, onion peeling and filtered back-projection methods

The Abel transform, onion peeling and FBP methods are the three commonly used reconstruction methods. The objective of the reconstruction or deconvolution is to find the spatial distribution f(r) based on the given projection p(l). Note that in Fig. 1 the radius r can be expressed in terms of l and s as $r = \sqrt{l^2 + s^2}$. Substituting s with r and l in Eq. (1) yields

$$p(l) = 2\int_l^\infty \frac{r\, f(r)}{\sqrt{r^2 - l^2}}\, dr \qquad (2)$$

Equation (2) provides an analytical expression for the projection function p(l), which turns out to be the Radon transform of the distribution function f(r) [11].

A well-known analytical inverse of Eq. (2) is the Abel transform [7],

$$f(r) = -\frac{1}{\pi}\int_r^\infty \frac{p'(l)}{\sqrt{l^2 - r^2}}\, dl \qquad (3)$$

The beauty of the Abel transform lies in its exactness and conciseness. Since the Abel transform is an exact solution to Eq. (2), it can in principle be calculated as accurately as desired. The accuracy of the results is limited by the numeric integration and noise in the raw projection data, p(l) when Eq. (3) is applied to experimental data.

The Abel transform is also unique. This can be deduced from the fact that f(r) ≡ 0, if p(l) ≡ 0. Based on this uniqueness, it is inferred that all the rigorous reconstruction methods must be equivalent to the Abel transform. This will be elaborated later in the discussion of the FBP method.

Equation (3) involves an improper integration because the integrand has a singularity at the lower integration limit and the upper integration limit approaches infinity. Strictly speaking, the convergence of the integration must be proven prior to attempting numerical calculations. However, when dealing with experimental data, it is impossible to discuss the convergence of the integration rigorously. Instead, the convergence of Eq. (3) is implicitly assumed with the physical nature of the quantity f(r) which exists in the experiment where the data of p(l) are collected.

The direct application of Eq. (3) has some disadvantages. Equation (3) requires calculating the derivative of projection data p(l), which are usually noisy. In addition, the results of the reconstruction may depend on the scheme for approximating the numerical derivative. For example, Dasch [12] employed different algorithms to calculate the derivatives of p(l) in his two-point and three-point Abel methods. The results obtained from the two

methods differ. To avoid the discrepancies caused by the derivative algorithms for p(l) and errors introduced by the derivative calculations, the following equation of the Abel transform is recommended:

$$f(r) = -\frac{1}{\pi}\int_r^\infty \frac{p(l)-p(r)}{(l^2-r^2)^{3/2}}\, l\, dl \qquad (4)$$

Equation (4) is rigorously equivalent to equation (3), but it uses the projection data directly instead of their derivative. It is noticed that the integrand in Eq. (4) also has a singularity at the lower integration limit. To overcome this difficult, it is recommended that the domain of integration is divided into two portions. The first portion covers the neighborhood of the lower integration limit, say from r to r+h while the second covers the remainder. Then, Eq. (4) is rewritten as:

$$f(r) = -\frac{1}{\pi}\int_r^{r+h} \frac{p(l)-p(r)}{(l^2-r^2)^{3/2}} l\, dl - \frac{1}{\pi}\int_{r+h}^\infty \frac{p(l)-p(r)}{(l^2-r^2)^{3/2}} l\, dl \qquad (5)$$

To resolve the difficulty caused by the singularity in the first integral in Eq. (5), the open type numeric integration formulas can be used, which do not evaluate the integrand at both ends of the integration domain. Steffensen's formulas [13] are good examples of the open type integration methods. The three point Steffensen's formula is used by the author to perform the numerical calculations for the examples presented later in this paper. It is also noticed that every set of experimental data is given in a finite domain, say l <L. For all l > L, p(l) = 0. Thus, the second term in Eq. (5) can be further simplified to yield:

$$f(r) = -\frac{1}{\pi}\int_r^{r+h} \frac{p(l)-p(r)}{(l^2-r^2)^{3/2}} l\, dl - \frac{1}{\pi}\int_{r+h}^{L} \frac{p(l)}{(l^2-r^2)^{3/2}} l\, dl + \frac{p(r)}{\pi\sqrt{h(2r+h)}} \qquad (6)$$

The second term in Eq. (6) can be evaluated using Simpson's rule since the integrand is regular over the entire domain. Therefore, Eq. (6) can be discretized directly with open type integration scheme and Simpson's rule or any other regular numerical integration formula. No attempt is made to present the entire discrete form of Eq. (6) in this paper. Interested readers may consult any popular books in numerical calculations to develop a suitable algorithm.

In contrast to the Abel transform, the onion-peeling method is completely based on numerical approximation. In the onion-peeling method, the entire domain of the spatial distribution is divided into a series of concentric rings, as shown in Fig. 2. Within each ring the value of the spatial function f(r) is assumed to be constant. Thus, Eq. (2) is approximated by the following summation:

$$p(l_i) = \sum_{j=i}^{\infty} s_{ij}\, f(\xi_j) \qquad r_j < \xi_j < r_{j+1} \qquad (7)$$

where s_{ij} is a matrix of the length of the i-th cord in the j-th ring which can be expressed as a function of l_i and ξ_j based on plane geometry. ξ_j is a selected radius in the j-th ring at which the value of the distribution function is considered to be the average over the j-th ring.

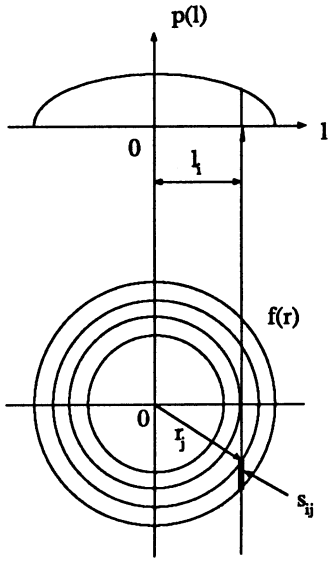

Figure 2. The Onion-peeling method. The entire reconstruction region is divided into a series of concentric rings.

Note that the coefficient matrix s_{ij} is independent of the projection p(l) and the distribution f(r). It can be calculated based on the arrangement of the dividing rings. Once s_{ij} is obtained, Eq. (7) can be solved for $f(\xi_j)$ by multiplying $p(l_i)$ with the inverse of the matrix s_{ij}:

$$f(\xi_j) = \sum_{i=j}^{\infty} [s_{ji}]^{-1}\, p(l_i) \qquad r_j < \xi_j < r_{j+1} \qquad (8)$$

It is obvious that when the width of each ring is infinitesimally small and the number of the rings approaches infinity, the results of onion-peeling method must approach the Abel transform. But, as the number of the rings increases, the difficulties and the amount of computational effort needed to invert the coefficient matrix s_{ij} increase rapidly. The number of basic executions (addition, subtraction or multiplication) needed to invert an N by N matrix is typically proportional to N^3, while that for the Abel transform, Eq. (6), is proportional to N. Therefore, if a large number of data points of p(l) need to be processed, the onion-peeling method becomes inefficient, not to mention the fact that the accumulative roundoff error increases with the number of executions.

The FBP method was developed by Ramachandran and Lakshminarayanan in 1971 [8] to perform two dimensional computed tomography (CT). The method was derived from the two dimensional Fourier transform method [14] which is an exact method based on the fact that a planar spatial distribution can be reconstructed by performing the two dimensional inverse Fourier transform of a series of one dimensional Fourier transforms of the projections of the distribution in various directions, i. e.,

$$F(R,\phi) = \int_{-\infty}^{\infty} p(l,\phi)\, e^{i2\pi Rl}\, dl \qquad (9)$$

and

$$f(r,\theta) = \int_0^{\infty} \int_0^{2\pi} F(R,\phi)\, e^{-i2\pi Rr\cos(\theta-\phi)} d\phi R\, dR \qquad (10)$$

where $p(l,\phi)$ is the projection at angle ϕ of a spatial distribution $f(r,\theta)$ defined in a polar coordinate system of r and θ, and R is the independent variable in the transform domain having unit of wave number per unit length. When a series of projections $p(l,\phi)$ are obtained from an experimental measurement, their Fourier transforms can be obtained per Eq. (9). Then the obtained Fourier transforms are substituted into Eq. (10) to yield the spatial distribution $f(r,\theta)$.

Ramachandran and Lakshminarayanan [8] showed that when both the projections $p(l,\phi)$ and the distribution $f(r,\theta)$ are spatially bandwidth limited, the Fourier transform method can be well approximated by a single convolution calculation in which the projections obtained in different directions are convoluted with a kernel function to yield the spatial distribution. This method is often referred to as back-projection method. Ramachandran and Lakshminarayanan's method adds some data filtering features to the Fourier transform method because the approximation made to derive the method eliminates the high frequency components, if present in the projections. The method was reported to give better reconstruction data than the Fourier transform method for certain testing sample functions [8]. The back-projection method significantly saves computing time in comparison with the Fourier transform method and has become popular in two dimensional reconstruction calculations.

Shepp and Logan [9] improved Ramachandran's method by proposing a new kernel function which is a weighted average of Ramachandran's kernel function over the two neighbor grid points of the grid point in calculation. Thus, Shepp and Logan's kernel function has more smoothing effect than Ramachandran's. This method is then referred to as filtered back projection method in some literature. Along the same line, Ravichandran and Gouldin [15] later proposed another kernel function derived from a "Kaiser" window instead of the Heaviside function and found the new kernel function generated better results for a distribution phantom than did the standard back-projection method.

Owing to its popularity in two dimensional tomography, the FBP method has been introduced to reconstruct axisymmetric spatial distributions by assuming identical projections obtained in all directions [3,5,10,12]. However, the FBP method is essentially the two dimensional Fourier transform method with a certain degree of data smoothing. Since both the two dimensional Fourier transform method and the Abel transform method are exact, it is inferred that when the former is applied to axisymmetric cases by assuming identical projections in all directions, i. e. $p(l,\phi) = p(l)$ in Eq. (9), it must yield the Abel transform. The detailed proof of this is presented in Appendix A. When FBP methods are applied to axisymmetric cases, the user must specify the number of projections, even though they are all assumed to be identical. In principle, the larger the number of the projections the more accurate the results. But, the user has to make a compromise between the accuracy and amount of the computing effort. It has been reported that assuming 40 to 100 identical projections is enough [3,5]. It is noticed that, as shown in Appendix A, the Abel transform actually implies infinite number of identical projections.

Therefore, in terms of accuracy, simplicity and rigor, the Abel transform is superior to both the onion-peeling method and the FBP method and should be the primary choice to reconstruct axisymmetric spatial distributions.

III. Spectral behavior of the Abel transform

It is often desirable to know how different wave number components in a projection contribute to the spatial distribution or vice versa. This leads to the study of the spectral relation between the projection and the spatial distribution. The Abel transform relates a projection to its corresponding distribution in the physical domain. It is used as the starting point to derive the spectral relation between the two in the spectral domain.

Multiplying both sides of Eq. (3) by $\cos(2\pi rv)\, dr$, then integrating from 0 to infinity with respect to r, and changing the order of integrations, we obtain the following equation relating the Fourier transform of a spatial distribution and that of the projection. A detailed derivation can be found in Appendix B.

$$F_f(v) = 2\int_v^{\infty} \frac{v_1 F_p(v_1)}{\sqrt{v_1^2 - v^2}}\, dv_1 \qquad (11)$$

where $F_f(v)$ and $F_p(v_1)$ are the Fourier transforms of f(r) and p(l), respectively, while v and v_1 are wave numbers in corresponding spectral domains. Note that since both p(l) and f(r) are even functions, their Fourier transforms are identical to their cosine transforms.

It is interesting to note that Eq. (11) resembles Eq. (2). F_p and F_f are in Eq. (11) as f(r) and p(l) in Eq. (2). It

immediately follows that the inverse of Eq. (11) must have the same form as Eq. (3). Thus,

$$F_p(\nu_1) = -\frac{1}{\pi}\int_{\nu_1}^{\infty} \frac{F_f'(\nu)}{\sqrt{\nu^2-\nu_1^2}}\, d\nu \qquad (12)$$

Eq. (12) shows that the Fourier transform of a projection is equal to the Abel transform of the Fourier transform of the corresponding spatial distribution. The interesting relations among the four functions are illustrated in Fig. 3.

Eqs. (11) and (12) unveil a number of interesting features of the Abel transform: first, from Eq. (11), the value of $F_p(\nu_o)$, where ν_o is a fixed wave number, contributes only to those $F_f(\nu)$ where ν is less than ν_o; second, if $F_p(\nu) \equiv 0$ for all $\nu > \nu_{max}$ (the maximum wave number for function F_p to be non-zero), $F_f(\nu) \equiv 0$ for all $\nu > \nu_{max}$ and vice versa. Based on the first feature, the component of a certain wave number in the distribution function is determined only by the components in the projection with higher wave numbers. The second feature indicates that for both the projection and the distribution, if one is bandwidth limited, the other is limited in the same bandwidth. Thus, we conclude that the bandwidth is unchanged by the Abel transform.

If p(l) and f(r) are not bandwidth limited, a necessary condition for Eqs. (11) and (12) to converge is that both $F_f(\nu)$ and $F_p(\nu)$ must approach zero as the wave number ν approaches infinity. In this case, it can be shown that the Abel transform has a bias towards high wave number components. Carrying out the integration in Eq. (11) for a function of $F_p = a\,\nu^{-n}$, where $n \geq 1$, yields that $F_f \sim \nu^{-(n-1)}$. This indicates that for large wave numbers, $F_p(\nu)$ descends at a rate of ν^{-n} while the corresponding $F_f(\nu)$ at a rate of $\nu^{-(n-1)}$, i.e., $F_p(\nu)$ descends faster than $F_f(\nu)$ with increasing wave numbers. Translating this to the physical domain we found that f(r) contains richer high wave number components than its projection function, p(l). This conclusion is consistent with the result of basic dimensional analysis. By inspection of Eqs. (2) and (3), it is noticed that the dimension of p(l) equals that of f(r) multiplied by a length dimension. Thus, converting f(r) to p(l) has a nature of integration, while the inverse, the Abel transform, has a nature of differentiation. Recall that integration of a function in physical domain corresponds to a division of its Fourier transform by the wave number in the Fourier domain. Thus integration results in attenuation of high wave number components, while differentiation does the opposite. This explains why differentiation normally exaggerates high wave number noises and integration tends to smooth noises out. Recall the fact that the Abel transform is unique and all the exact reconstruction methods are equivalent to it. We therefore conclude that all the exact reconstruction methods are sensitive to high frequency components including noises. Therefore, it is not surprising to have rugged or noisy reconstruction results of fairly smooth input projections when the Abel transform or the two dimensional Fourier transform method are used. If high wave number noises are found to be a problem, a low-pass filter should be used to remove or reduce those noises prior to the reconstruction calculations.

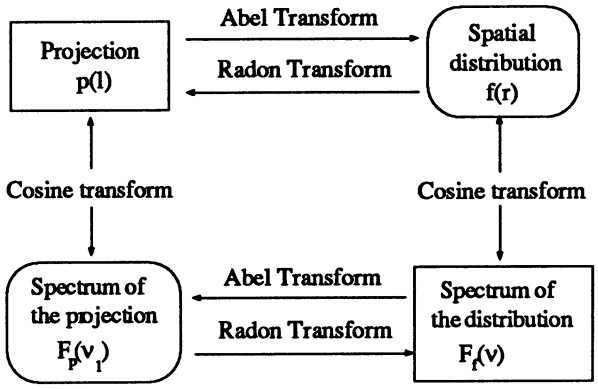

Figure 3. The relations among a spatial distribution, its projection and their spectrums.

IV. The filtered Abel transform

It is almost inevitable to apply some sort of filters to the experimental data to reduce noises before performing reconstruction. Filtering and reconstruction usually are two separate steps in experimental data reduction. In this paper, a new method, the filtered Abel transform, is developed which combines filters with the Abel transform.

Applying a filter to a projection can be carried out in the Fourier domain by multiplying the spectrum of the projection by the response function of the filter. Then the resulting spectrum is converted to the physical domain to yield the filtered projection. Denoting the spectrum of the filtered projection by $F_{pf}(\nu)$, we have

$$F_{pf}(\nu) = F_p(\nu)\cdot G(\nu) \qquad (13)$$

where $G(\nu)$ is the response function of the filter. By the convolution theorem, the counterpart of Eq. (13) in the physical domain is

$$p_f(l) = \int_{-\infty}^{\infty} p(\lambda)\, g(l-\lambda)\, d\lambda \qquad (14)$$

where $p_f(\lambda)$ is the filtered projection and g(l) is the filtering function, the inverse Fourier transform of the response function $G(\nu)$. Since the projection p(l) of an axisymmetric distribution is always an even function, Eq. (14) can be rewritten as:

$$p_f(l) = \int_0^{\infty} p(\lambda)\,[\, g(l+\lambda) + g(l-\lambda)\,]\, d\lambda \qquad (15)$$

The function in the bracket will be referred to as the filtering kernel function later in this paper. The Abel transform of the filtered projection $p_f(l)$ is

$$f(r) = -\frac{1}{\pi}\int_r^\infty \frac{1}{\sqrt{l^2-r^2}} \left\{ \int_0^\infty p(\lambda) \frac{d[\, g(l+\lambda)+g(l-\lambda)\,]}{d\,l}\, d\lambda \right\} dl \qquad (16)$$

By changing the order of the integrations, we have

$$f(r) = -\frac{1}{\pi}\int_0^\infty p(\lambda) \left\{ \int_r^\infty \frac{[\, g(l+\lambda)+g(l-\lambda)\,]'_l}{\sqrt{l^2-r^2}}\, dl \right\} d\lambda \qquad (17)$$

It is noticed that the inner integration in Eq. (17) is the Abel transform of the filtering kernel function in Eq. (15). By defining a new kernel function $M(\lambda,r)$ in the following manner:

$$M(\lambda, r) = -\frac{1}{\pi}\int_r^\infty \frac{[\, g(l+\lambda)+g(l-\lambda)\,]'_l}{\sqrt{l^2-r^2}}\, dl \qquad (18)$$

Eq. (17) can be rewritten as:

$$f(r) = \int_0^\infty p(\lambda)\, M(\lambda, r)\, d\lambda \qquad (19)$$

Eqs. (18) and (19) are referred to as the filtered Abel transform. To implement this method, the kernel function $M(\lambda,r)$ is obtained first as the Abel transform of a desired filter. As recommended before, the Abel transform can be carried out with Eq. (6). Then, an integral transform of the projection data with the kernel function $M(\lambda,r)$ is performed to yield the spatial distribution as described in Eq. (19). Since the kernel function $M(\lambda,r)$ is independent of the projection, it can be calculated separately. The method itself is not associated with any particular filters. Users can select different filters for a particular set of experimental data to get the best results. After the kernel function $M(\lambda,r)$ is obtained, it can be used repeatedly, for instance, if a full flame image needs to be processed where each row is a projection of a cross section of the flame. In this case, the same kernel function $M(\lambda,r)$ can be used for all the projections to reconstruct the entire spatial distribution of the flame.

The following are two commonly used low pass filtering functions. The rectangular response function in the Fourier domain is

$$G(\nu) = \begin{cases} 1, & |\nu| \le \nu_b; \\ 0, & |\nu| > \nu_b. \end{cases} \qquad (20)$$

where ν_b is the cut-off wave number of the filter. The corresponding kernel function in the physical domain is

$$g(l) = \frac{\sin(2\pi\nu_b l)}{\pi\, l} \qquad (21)$$

This filter cuts off all the components with wave number higher than ν_b. Another example of low pass filters has a rectangular window in the physical domain. The two functions of this filter are

$$G(\nu) = \frac{\sin(2\pi l_b \nu)}{\pi\, \nu} \qquad (22)$$

and

$$g(l) = \begin{cases} 1, & |l| \le l_b; \\ 0, & |l| > l_b. \end{cases} \qquad (23)$$

where l_b is the width of the rectangular window. This filter replaces the projection value at a given point with the average value of the projection over the width of the window. Many other low-pass filters are available and can be used with the filtered Abel transform method.

Finally, it is noticed that the order of the data filtering process and the Abel transform are not changeable. Performing the Abel transform on the projection data, then filtering the results yield different results from filtering the projection data first followed by the Abel transform. This can be shown with a few steps of derivation from Eqs. (14) or (15). Since the major error sources are in the raw experimental data, not in the reconstruction algorithms, the correct procedure is to filter the projection data first, then perform the Abel transform. The filtered Abel transform method is derived in compliance with this sequence although the selected filter is not directly applied to the projection data.

V. Examples

A computer code has been developed to deconvolute two dimensional flame images with the filtered Abel transform. The two filters described by Eqs. (21) and (23) are included as built-in filters for users to select. The code also has an option of direct Abel transform without data filtering. Equation (6) is employed to perform the Abel transform on the selected filtering function or directly on the projection data when no filtering is selected. The three point Steffensen's method followed by Simpson's rule is used to implement Eq. (6).

A projection of a unit distribution function within a circle with radius of 0.5 is used to test the code. It is noticed that the unit distribution is very difficult to reconstruct because of the discontinuity at the edge of the distribution which contains rich high wave number

components. However, testing a reconstructon method against a unit distributon function has a fundamental significance since all the reconstructon methods are linear operations and any distributon functions can be considered as the linear combinatons of unit distributions with various radii. Figure 4 shows the unit distribution function (labeled as True value in the plot), its projection and the reconstructed distribution with the Abel transform without data filtering.

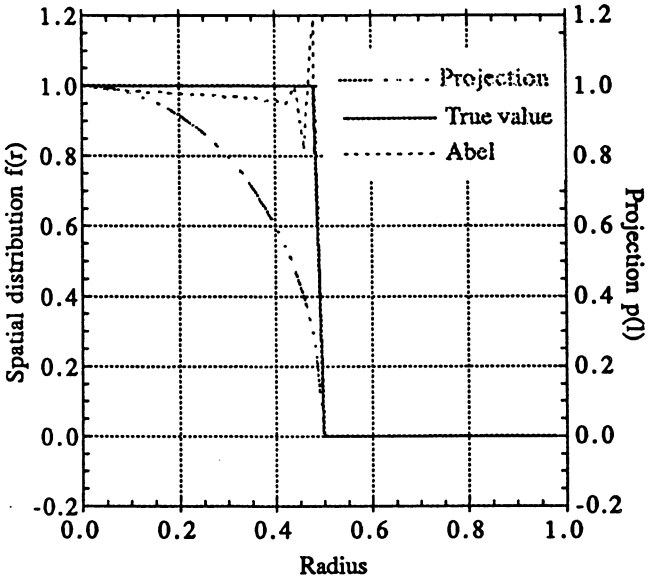

Figure 4. The reconstructed spatial distribution of a unit testing distribution with the Abel transfrom.

A total of 50 data points are used across the entire domain of the independent variable l or r. The reconstructed distribution agrees well with the original distribution in the most region except for the neighborhood of r = 0.5 where a sudden change occurs in the original distribution function and the derivative of the projection approaches infinity. The overall mean-square error of the reconstructed distribution is 0.041 including the overshoot points.

Three other reconstructed distributions for the same projection as in Fig. 4 are presented in Fig. 5. They are generated with the filtered Abel transform with the filtering function being described in Eq. (23). The three reconstructed distributions, labeled with fAbel2/1, fAbel2/2 and fAbel2/3 in the plot, are corresponding to three different widths of the filter window (l_o = 1, 2, 3). It can be seen that the filter significantly reduces the overshoot of the reconstructed function at the sharp edge of the original distribution. In principle, it is impossible to remove the fluctuations of the reconstructed distribution completely if the original distribution is not bandwidth limited. When the integrals in Eq. (6) are discretized, the integrand is evaluated at a finite number of points, i.e., at the integration grid points. Detailed information of the integrand within integration grids is lost. The contributions from components with wave number greater than one over the length of two grids are folded to their counterpart with "mirror" wave numbers. This phenomenon is called aliasing. In Fig. 5, the reconstructed distributions show different slopes at the sharp edge of the original distribution, because the filters suppress the high wave number components to different extents depending on the width of the filter. The wider the filtering window the smoother the reconstructed distribution, but the poorer the response of the reconstructed distribution to the rapid change in the original distribution. The overall mean-square error of the three reconstructed distributions are 0.086, 0.101 and 0.119 for l_o being 1, 2, 3, respectively.

Although the direct Abel transform yields the smallest overall mean square error among the four reconstructed

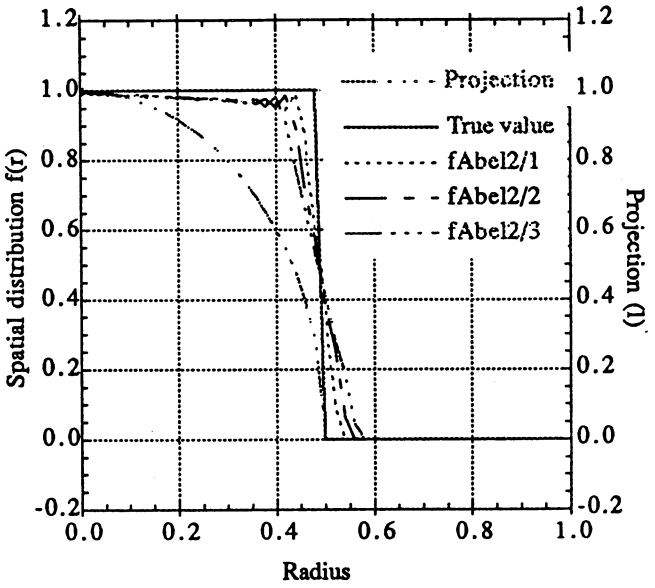

Figure 5. The reconstructed spatial distribution of a unit testing distribution with the filted Abel transfrom

distributions, it generates a cosiderable overshoot at the falling edge of the distribution data. It is noticed that the filtered Abel transform with a window width of 1 seems to be the best compromise between the overall and the local reconstruction of the original distribution.

Figure 6 shows a laser extinction image for soot volume fraction measurement of a Burke-Schumann flame. Propylene was used as the fuel gas supplied at 80 sccm. The rate of the co-flow air was 30 SLPM. The inner diameter of the burner was 14.29 mm. A laser beam generated by a 634 nm diode laser source was expanded and collimated with a parabolic mirror to cover the whole flame area. After the collimated laser passed the flame, it was decollimated and the image of extinction was collected by a CCD camera. The darkened center portion in Fig. 6 shows the reduced laser intensity due to the absorption of the soot particles inside or above the flame. At the test flow rate, the propylene flame exceeded the smoke height so that the soot emitted from the flame extends beyond the field of view. The total extinction of a single laser ray is proportional to

the line-of-sight integration of the spectral absorption coefficient of the soot particles [16]. The soot volume fraction is calculated based on the following equation:

$$f = \frac{\lambda}{6\pi E} A\left\{ \ln\left(\frac{I_o}{I_s}\right)\right\} \qquad (24)$$

where λ is the wavelength of the laser beam, E is a constant of 0.2595 determined by the optical properties of soot particles, I_o and I_s are the laser intensities of the background and soot image, respectively. The symbol A{ } denotes a reconstruction operator, i.e., the filtered Abel transform in this paper.

A section of the image from 13.3 mm through 27.8 mm above the burner tip, as shown in Fig. 6, was selected to perform soot volume fraction calculation. This section includes 100 pixels streamwise and 69 pixels cross the flame. Three different deconvolution methods were used in the calculation, the direct Abel transform, the filtered Abel transform with a filter with the window width of 1 and that with the window width of 3. The results are presented in Fig. 7. Figures 8 and 9 show the same results at two cross sections of the flame. The results from all the three methods show that the soot was concentrated in a soot shell close to the outer visible boundary of the flame. At the bottom of the plotted area, the soot shell has larger diameter, but lower peak value, in comparison with the top portion of the plotted area as shown in Figs. 8 and 9.

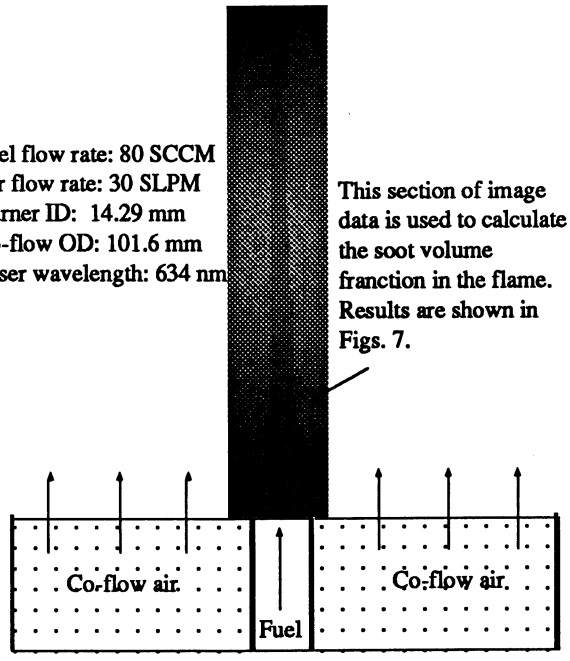

Figure 6. The laser extinction image for soot volume fraction measurement of a propylene diffusion flame with co-flow air.

The plot on the right side of Fig. 7 shows the results from direct Abel transform without data filtering. The obtained soot volume fraction data fluctuate in a wide range (also see Figs. 8 and 9). The peak value reaches as high as 120 ppm, which is within the saturated dark region of the plot. The scale of the plot is set from 0 to 40 ppm to have the best resolution over the most part of the flame. The random soot distribution outside the frame region is unreal and resulted from the noise in the background and the extinction images. The plots at the center and the left of Fig. 7 show the results of the same flame section from filtered Abel transform with filter window width being 1 and 3, respectively. The differences among the three plots indicate that the more the filtering the smoother the results and the lower the peak values. In general, it is difficult to determine the best level of data smoothing based only on the laser extinction images. From the results of above unit distribution test, it is reasonable to consider the plot in the middle of Fig. 7 gives the best result among the three. However, it is suggested that the results from other relevant experiments, if available, should be considered together with the laser extinction measurements to yield comprehensive interpretation of the soot concentration in a flame.

VI. Summary

Because of the exactness and the uniqueness of the Abel transform, all exact deconvolution methods for axisymmetric distributions are shown to be equivalent to the Abel transform. In axisymmetric cases, the spatial distributions and their projections have the same bandwidth if they are bandwidth limited. The Abel transform has a bias towards high wave number components, if the spatial distribution and the projection are not bandwidth limit. This is also true for all exact deconvolution methods, since they are equivalent to the Abel transform. Because of this, the importance of data filtering is more pronounced when experimental data need to be deconvoluted. The filtered Abel transform provides users with the flexibility of applying various filtering functions and it also speeds up the deconvolution process when a large number of projection lines needs to be processed. Further study of the reconstruction of axisymmetric distribution includes trying different numerical integration schemes in Eq. (6) to optimize the algorithm, and testing various filtering functions for known distributions.

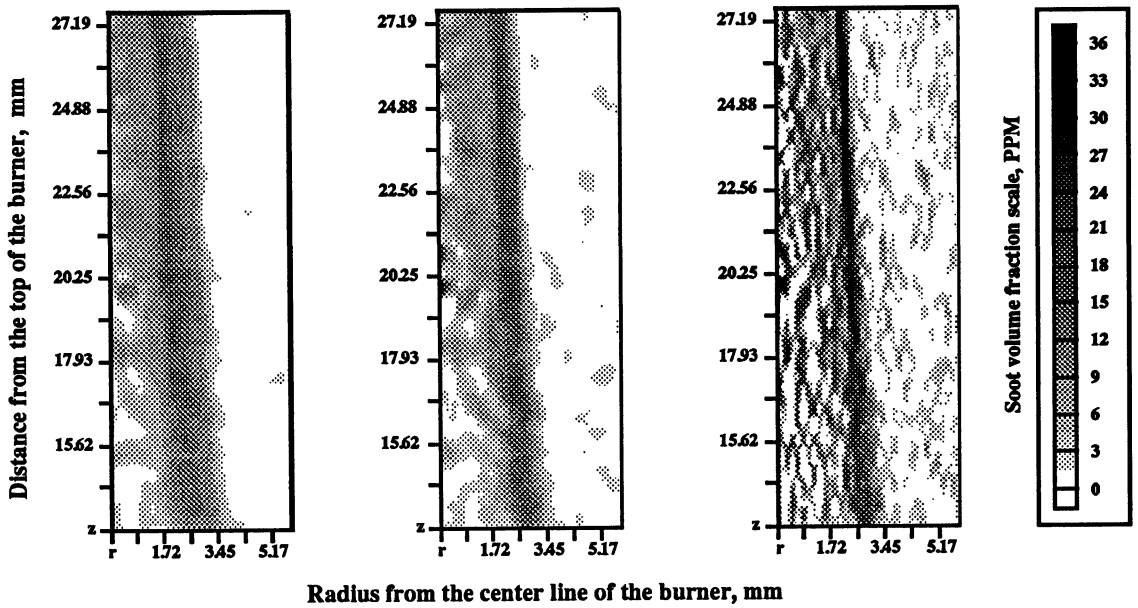

Figure 7. The soot volume fraction in the section of the propylene flame shown in Fig. 6. The right-most plot shows the results of direct Abel transform without data filtering, while the left-most plot and the center one are from the fitered Abel transform with filtering window width of 3 and 1, respectively.

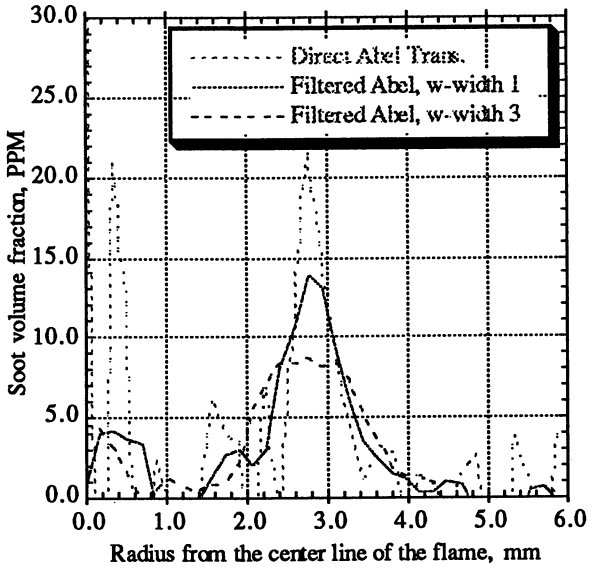

Figure 8. Soot volume fraction distribution obtained with different data filtering parameters at a cross section of the flame 13.5 mm above the burner tip.

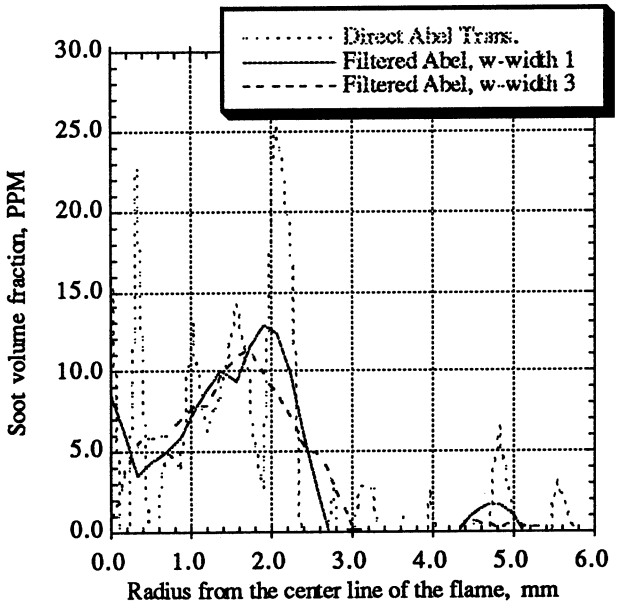

Figure 9. Soot volume fraction distribution obtained with different data filtering parameters at a cross section of the flame 27.6 mm above the burner tip.

Appendix A

In this Appendix, it is shown that the when the two dimensional Fourier Transform method is applied to a one dimensional axisymmetric problems, it leads to the Abel Transform. For axisymmetric problems, the projections are independent of direction ϕ. Since the projection p(l) must be a even function, Eq. (9) in the main text becomes

$$F(R,\phi) \equiv F(R) = 2\int_0^\infty p(l)\cos(2\pi Rl)\,dl \tag{1a}$$

Using integration by parts and invoking the boundary condition that p(∞) -> 0, we have:

$$-\frac{1}{\pi R}\int_0^\infty p'(l)\sin(2\pi Rl)\,dl = 2\int_0^\infty p(l)\cos(2\pi Rl)\,dl$$

$$= F(R) \tag{2a}$$

On the other hand, the two dimensional Fourier Transform, Eq. (10) in the main text, and its inverse are reduced to the Hankel Transform pair when f(r) is a function of r only in a polar coordinate system:

$$F(R) = \int_0^\infty r f(r) J_0(2\pi Rr)dr \tag{3a}$$

and

$$f(r) = \int_0^\infty R F(R) J_0(2\pi Rr)dR \tag{4a}$$

where J_0 is the zero order first kind Bessel function. Substituting Eq. (2a) into (4a) yields

$$f(r) = -\frac{1}{\pi}\int_0^\infty J_0(2\pi Rr)\int_0^\infty p'(l)\sin(2\pi Rl)\,dl\,dR \tag{5a}$$

By changing the order of integrations, Eq. (5a) can be rewritten as:

$$f(r) = -\frac{1}{\pi}\int_0^\infty p'(l)\int_0^\infty \sin(2\pi Rl)J_0(2\pi Rr)\,dR\,dl \tag{6a}$$

The inner integration is independent of p'(l) and can be carried out separately yielding:

$$\int_0^\infty \sin(2\pi Rl)J_0(2\pi Rr)\,dR = \begin{cases} \frac{1}{\sqrt{l^2-r^2}} & l>r \\ 0 & l<r \end{cases} \tag{7a}$$

Substituting Eq. (7a) into (6a) gives

$$f(r) = -\frac{1}{\pi}\int_r^\infty \frac{p'(l)}{\sqrt{l^2-r^2}}\,dl \tag{8a}$$

Equation (8a) the very form of the Abel Transform.

Appendix B

In this Appendix the detailed derivation of the spectral form of the Abel transform is presented. Start with Eq. (3), the Abel transform, in the main text and denote the Cosine transform of f(r) with $F_f(\nu)$ and that of p(l) with $F_p(\nu_1)$ where ν and ν_1 are the wave numbers, the independent variables, in the two Fourier domains. Since f(r) must be an even function, we have

$$F_f(\nu) = 2\int_0^\infty f(r)\cos(2\pi r\nu)\,dr = \int_{-\infty}^\infty f(r)\,e^{i2\pi r\nu}\,dr \tag{1b}$$

Substituting f(r) of Eq. (3) into Eq. (1b) yields

$$F_f(\nu) = \int_{-\infty}^\infty \left[-\frac{1}{\pi}\int_r^\infty \frac{p'(l)}{\sqrt{l^2-r^2}}\,dl\right]e^{i2\pi r\nu}\,dr \tag{2b}$$

Define a kernel function in the following manner:

$$k(l,r) = \begin{cases} 0, & l<r \\ \frac{1}{\sqrt{l^2-r^2}}, & l\geq r \end{cases} \tag{3b}$$

Substituting Eq. (3b) into (2b) and changing the order of the integrations in Eq. (2b) yields

$$F_f(\nu) = -\frac{1}{\pi}\int_0^\infty p'(l)\left[\int_{-\infty}^\infty k(l,r)\,e^{i2\pi r\nu}\,dr\right]dl \tag{4b}$$

The inner integral can be carried out as follows.

$$\int_{-\infty}^\infty k(l,r)e^{i2\pi r\nu}dr = 2\int_0^\infty k(l,r)\cos(2\pi r\nu)dr = \pi J_0(2\pi l\nu) \tag{5b}$$

Substituting Eq. (5b) into Eq. (4b), we have

$$F_f(\nu) = -\int_0^\infty p'(l)\,J_0(2\pi l\nu)\,dl \tag{6b}$$

On the other hand, since $F_p(\nu_1)$ is the Cosine transform of p(l), the inverse of the cosine transform gives:

$$p(l) = 2\int_0^\infty F_p(\nu_1)\cos(2\pi l\nu_1)\,d\nu_1 \tag{7b}$$

Taking derivatives with respect to l on both sides of Eq. (7b), we have

$$p'(l) = -4\pi \int_0^\infty \nu_1 F_p(\nu_1) \sin(2\pi l \nu_1)\, d\nu_1 \qquad (8b)$$

Substituting Eq. (8b) into (6b) and changing the order of the integrations, we have

$$F_f(\nu) = 4\pi \int_0^\infty \nu_1 F_p(\nu_1) \int_0^\infty \sin(2\pi l \nu_1)\, J_0(2\pi l \nu)\, dl\, d\nu_1 \qquad (9b)$$

The inner integral in Eq. (9b) can be carried out as follows.

$$\int_0^\infty \sin(2\pi l \nu_1)\, J_0(2\pi l \nu)\, dl = \begin{cases} 0, & \nu_1 < \nu \\ \dfrac{1}{2\pi\sqrt{\nu_1^2 - \nu^2}}, & \nu_1 \geq \nu \end{cases} \qquad (10b)$$

Substituting Eq. (10b) into (9b), we have

$$F_f(\nu) = 2 \int_\nu^\infty \frac{\nu_1 F_p(\nu_1)}{\sqrt{\nu_1^2 - \nu^2}}\, d\nu_1 \qquad (11c)$$

Equation (11b) is identical to Eq. (11) in the main text.

References

1. P.J.Emmerman, R.Goulard, R.J.Santoro and H.G.Semerjian, "Multiangular Absorption Diagnostics of a Turbulent Argon-Methane Jet," J. Energy, Vol. 4, No.2, Article No. 79-0085R, pp. 70-77, March-April 1980.

2. R.J.Santoro, H.G.Semerjian, P.J.Emmerman and R.Goulard, "Optical Tomography for Flow Field Diagnostics," Int. J. Heat Mass Transfer, Vol. 24, No. 7, pp. 1139-1150, 1981.

3. R.J.Santoro, H.G.Semerjian and R.A.Dobbins, "Soot Particle Measurements in Diffusion Flames," Combustion and Flame, Vol. 51, pp. 203-218, 1983.

4. Hiroki Uchiyama, Masato Nakajima and Shinichi Yuta, "Measurement of flame temperature distribution by IR emission computed tomography," Applied Optics, Vol. 24, No. 23, pp. 4111-4116, Dec. 1985.

5. R.J.Hall and P.A.Bonczyk, "Sooting flame thermometry using emission/absorption tomography," Applied Optics, Vol. 29, No. 31, Nov. 1990.

6. P.S.Greenberg,"Laser Doppler Velocimetry and Full-Field Soot Volume Fraction Measurements in Microgravity," presented at Third International Microgravity Combustion Workshop, Cleveland, Ohio, April 11-13, 1995.

7. N.H.Abel, "Auflosung einer mechanischen Aufgabe," J. fur die Reine & Angew. Math.Vol. 1, 153-157(1826).

8. G.N.Ramachandran & A.V.Lakshminarayanan, "Three-dimensional Reconstruction from Radiographs and Electron Micrographs: Application of Convolutions instead of Fourier Transforms," Proc. Nat. Acad. Sci. USA., Vol. 68, No. 9, pp. 2236-2240, Sept. 1971.

9. L.A.Shepp and B.F.Logan, "The Fourier Reconstruction of a Head Section," IEEE Transactions on Nuclear Science, Vol. NS-21, pp. 21-43, June 1974.

10. B.J.Hughey and D.A.Santavicca, "A Comparison of Techniques for Reconstructing Axisymmetric Reacting Flow Fields from Absorption Measurements," Combustion Science and Technology, Vol. 29, pp. 167-190, 1982.

11. Johann Radon, "Über die Bestimmung von Funktionen durch ihre Integralwerte längs gewisser Mannigfaltigkeiten," Berichte Sächsische Akademie der Wissenschaften. Leipzig, Math.--Phys. Kl., Vol. 69, pp.262-267, 1917.

12. Cameron J. Dasch, "One-dimensional tomography: a comparison of Abel, onion-peeling, and filtered backprojection methods," Applied Optics, Vol. 31, No. 8, March 1992.

13. Philip J. Davis and Philip Rabinowitz, "Methods of Numerical Integration," Academic Press, 1975, pp. 70- 71.

14. D. W. Sweeney and C. M. Vest, "Reconstruction of three-dimensinal refractive index fields from multidirectional interferometric data," Applied Optics, Vol. 12, No. 11, 1973.

15. M. Ravichandran and F. C. Gouldin, "Reconstruction of smooth distributions from alimited number of projections," Applied Optics, Vol. 27, No. 19, 4084, 1988.

16. Robert Siegel and John R. Howell, "Thermal Radiation Heat Transfer", 2nd ed., McGraw-Hill , pp. 450-595.

REPORT DOCUMENTATION PAGE

Form Approved
OMB No. 0704-0188

1. AGENCY USE ONLY (*Leave blank*)	2. REPORT DATE	3. REPORT TYPE AND DATES COVERED
	March 2003	Final Contractor Report

4. TITLE AND SUBTITLE

The Filtered Abel Transform and Its Application in Combustion Diagnostics

5. FUNDING NUMBERS

WBS–22–101–52–01
NCC3–975

6. AUTHOR(S)

Zeng-Guang Yuan

7. PERFORMING ORGANIZATION NAME(S) AND ADDRESS(ES)

National Center for Microgravity Research
21000 Brookpark Road
Cleveland, Ohio 44135

8. PERFORMING ORGANIZATION REPORT NUMBER

E–13773

9. SPONSORING/MONITORING AGENCY NAME(S) AND ADDRESS(ES)

National Aeronautics and Space Administration
Washington, DC 20546–0001

10. SPONSORING/MONITORING AGENCY REPORT NUMBER

NASA CR—2003-212121

11. SUPPLEMENTARY NOTES

Prepared for the 1995 Fall Meeting, Western States Section sponsored by the Combustion Institute, Stanford, California, October 30–31, 1995. Project Manager, Stephen N. Simons, Microgravity Science Division, NASA Glenn Research Center, organization code 6700, 216–433–5277.

12a. DISTRIBUTION/AVAILABILITY STATEMENT

Unclassified - Unlimited
Subject Categories: 64 and 74 Distribution: Nonstandard

Available electronically at http://gltrs.grc.nasa.gov

This publication is available from the NASA Center for AeroSpace Information, 301–621–0390.

12b. DISTRIBUTION CODE

13. ABSTRACT ***(Maximum 200 words)***

Abel transform is widely used for deconvoluting data acquired from an axisymmetric domain with noninstrusive diagnostic methods. This paper shows the Abel transform is more efficient than other deconvolution methods for axisymmetric case. An algorithm is presented to perform Abel transform that differs from conventional algorithm which needs to calculate the derivatives of the raw data. By eliminating derivative calculation, the proposed algorithm not only runs faster, but also avoids errors from derivative calculations. It is also demonstrated that data filtering procedures can be incorporated in the Abel transform, making it particularly efficient when multiple data sets obtained with the same instrumentation needs to be processed, as often encountered in a three-dimensional tomography. An example of using the filtered Abel transform to obtain the soot volume fraction is given at the end of the paper.

14. SUBJECT TERMS

Abel transform; Deconvolution; Laser; Diagnostics

15. NUMBER OF PAGES

17

16. PRICE CODE

17. SECURITY CLASSIFICATION OF REPORT	18. SECURITY CLASSIFICATION OF THIS PAGE	19. SECURITY CLASSIFICATION OF ABSTRACT	20. LIMITATION OF ABSTRACT
Unclassified	Unclassified	Unclassified	